


General framework for two-photon spontaneous emission near plasmonic nanostructuresS. Smeets^{*,†}, B. Maes[‡], and G. Rosolen[‡]*Micro- and Nanophotonic Materials Group, Research Institute for Materials Science and Engineering, University of Mons, 20 Place du Parc, Mons B-7000, Belgium* (Received 24 February 2023; accepted 6 June 2023; published 27 June 2023)

We present a general framework that computes the two-photon spontaneous emission rate of a quantum emitter close to an arbitrary photonic structure beyond the dipolar approximation. This is relevant for strongly confined light fields, such as in plasmonic nano- and picocavities, which are currently being explored to enhance higher-order light-matter interactions. In our framework, the emitter contribution to this process is calculated analytically, while the influence of the photonic environment is determined via the computation of Purcell factors with conventional electromagnetic simulations, which avoids tedious analytic calculations for the environment. Also, our framework efficiently handles asymmetric structures that were not treated before. We show that placing a hydrogen-like emitter close to a silver nanodisk enhances the transition rate between two spherically symmetric states by 5 and 11 orders of magnitude via electric dipole and quadrupole two-photon transitions, respectively. In the future, controlling this process promises efficient entangled two-photon sources for quantum applications, new platforms in spectroscopy, as well as broadband absorbers and emitters.

DOI: [10.1103/PhysRevA.107.063516](https://doi.org/10.1103/PhysRevA.107.063516)**I. INTRODUCTION**

Spontaneous emission, which is responsible for most of the light we see around us, is a fundamental process in the field of light-matter interaction. In this process, an excited quantum emitter (e.g., an atom, a molecule, or a quantum dot) decays into a lower energy state by emitting a quantized amount of energy in the form of a single quantum or in the form of several quanta [1–3]. These transitions are also responsible for the fingerprint of atoms and molecules, which is their emission spectrum [4].

Nowadays, it is well known that the spontaneous emission rate of an emitter does not depend only on the emitter itself but also on its environment, termed the Purcell effect [5,6]. Moreover, an excited emitter can decay either radiatively in the case of photon emission in the far field or nonradiatively in the case of energy dissipation in the environment in the form of, for example, phonons or plasmons [6]. Especially near metallic structures, the two relaxation channels can be enhanced [7], and in many applications one aims to harness the radiative one.

Usually, because the size of a quantum emitter is typically three orders of magnitude smaller than the wavelength of the emitted light, it is sufficient to study the influence of the environment on the emitter under the electric dipole approximation [6,8]. In the latter approach the emitter feels a uniform electric field, thus neglecting the spatial variations of the field over it. Therefore, the emitter is assumed to be a point and

only electric dipole transitions can occur [9], making most of the characteristic emitter transitions inaccessible [10].

Nevertheless, when the spatial extent of an emitter is no longer negligible compared with the wavelength of light, the point dipole approximation is no longer valid. This can happen with emitters having a large spatial extent, such as quantum dots or organic molecules [11–14] and in current devices used to increase light-matter interactions [15] where the light can be highly confined, such as photonic crystals [16,17], plasmonic nanocavities [11,18–22], nanomagnonic cavities [23,24], and polar dielectrics [25,26]. For example, the wavelength can be squeezed by two orders of magnitude in the form of localized surface plasmons and, therefore, the spatial variation of the fields over an emitter is no longer negligible [10,27–30]. Furthermore, the breakdown of the electric dipole selection rule leads to a multitude of “forbidden” transitions becoming accessible, which can compete with the one-photon electric dipole transition: the multipolar processes, multiquanta emission processes, and spin-flip processes [10,15,30].

In this article we focus on the two-photon spontaneous emission (TPSE) process that is typically 8 to 10 orders of magnitude slower than the competing spontaneous emission of a single photon [10]. Historically this second-order process in perturbation theory was predicted by Göppert-Mayer in 1931 [31]. It is the main process responsible for the mean lifetime of the $2s$ state of hydrogen [32], which is at the origin of the continuous spectrum coming from planetary nebulae [33]. The first estimate of this two-electric dipole transition rate was made by Breit and Teller in 1940 [32], and one decade later Spitzer and Greenstein realized a refinement and found a value of 8.23 s^{-1} [33]. It was not until 1975 that the first experimental measurement of the two-photon emission rate in hydrogen was carried out [34]. In 1981 Goldman and

*Steve.Smeets@umons.ac.be

†Bjorn.Maes@umons.ac.be

‡Gilles.Rosolen@umons.ac.be

Drake realized the first calculations that include multipolar contributions to the TPSE process [35]. For the hydrogen atom they found that the two magnetic dipole and the two electric quadrupole transition rates are, respectively, 12 and 13 orders of magnitude smaller than the two electric dipole one. More recently the TPSE process has been investigated in systems other than hydrogen, such as in quantum dots [17,36], semiconductors [37–40], and epsilon-near-zero-materials [41].

Nowadays interest in the tailoring of this process grows [40,42] as it has several applications [43]. For example, it promises efficient entangled photon sources for quantum applications [37,44,45], it allows spectroscopy to access a usually invisible part of a spectrum [44], and it leads to the conception of broadband absorbers and light emitters since this is a continuous process [46]. However, the current study of TPSE near arbitrary objects is hampered by a lack of efficient theoretical and numerical methods.

A few years ago, Muniz *et al.* derived an expression for the TPSE transition rate of a quantum emitter as a function of the one-photon Purcell factors, with the restriction that structures are symmetric, that the emitter is at specific positions, and under the electric dipole approximation [47]. With an analytical calculation of these factors they studied the two-photon Purcell effect near two-dimensional (2D) plasmonic nanostructures, ideal to harness TPSE from single emitters [48].

In this paper we present an efficient and more general framework that computes the TPSE rate of a quantum emitter at any position, close to an arbitrary structure, and beyond the dipolar approximation, i.e., by taking into account the electric dipole, magnetic dipole, and electric quadrupole contributions, respectively, which is relevant for state-of-the-art current plasmonic nanostructures [10,27–30] and for larger emitters [11–14]. Note that our framework is based on the Fermi's golden rule and is therefore limited to the weak-coupling regime. Indeed, the perturbation theory is expected to fail when the ratio between the one-photon spontaneous emission rate and the transition angular frequency approaches one [10]. Furthermore, for the extreme cases of large emitters placed very close to a nanostructure (≈ 1 nm distance), the point approximation fails and one needs to consider the spatial extent of the emitter [14].

To this end in Sec. II we start with Fermi's golden rule to provide the multipolar emission channel contributions to the TPSE rate. In Sec. III, via the expression of the rates in terms of the dyadic Green's function, we establish for each multipolar contribution the connection between the TPSE rate and the one-photon Purcell factors. In Sec. IV our framework is applied to study the modification of the TPSE rate of a hydrogen-like emitter placed near a plasmonic silver nanodisk, also in an asymmetric configuration that was not handled before. The document ends with a conclusion in Sec. V. Throughout this document we refer several times to our Supplemental Material [49], which provides more details.

II. MULTIPOLAR EMISSION CHANNEL CONTRIBUTIONS TO THE TWO-PHOTON SPONTANEOUS EMISSION PROCESS

In this section we discuss the contribution of the two electric dipole, two magnetic dipole, and two electric quadrupole

emission channels to the TPSE process. For this purpose Fermi's golden rule is reminded because it is used to calculate the transition rates, and we introduce the states involved in this second-order process. Then we present the Hamiltonian that describes the emitter-field interactions, and the electromagnetic field operators are given. Finally, we provide the multipolar emission channel contributions to the TPSE rate and describe the particular case where the environment of the emitter is vacuum.

A. Fermi's golden rule

Let us consider a system composed of a quantum emitter (e.g., an atom, a molecule, or a quantum dot) and its photonic environment. With a perturbative approach the probability per unit time that the system carries out a second-order transition by emitting two quanta from an initial state $|i\rangle$ to a final state $|f\rangle$, upon an interaction described by the Hamiltonian H_{int} , is given by Fermi's golden rule [2,50]

$$\Gamma_{i \rightarrow f}^{(2)} = \frac{2\pi}{\hbar} |M_{fi}^{(2)}|^2 \delta(E_f - E_i), \quad (1)$$

with the second-order matrix element

$$M_{fi}^{(2)} = \sum_l \frac{\langle f | H_{\text{int}} | l \rangle \langle l | H_{\text{int}} | i \rangle}{E_i - E_l}, \quad (2)$$

where the summation runs over all possible virtual intermediate states $|l\rangle$ of the system. In these equations \hbar is the reduced Planck constant, E_a stands for the energy of the system in the state $|a\rangle$ with $a = i, l, f$, and the superscript (2) indicates that this is a second-order transition. Furthermore, this second-order transition can be seen as two successive transitions in which each one emits a quantum.

Regarding the states in this second-order process [50], the initial one is characterized by the emitter in an excited state $|e\rangle$ and the field in the vacuum state $|\text{vac}\rangle$, while in the final state the emitter is in a lower energy state $|g\rangle$ and the field is in a two-quanta state $|1_\alpha, 1_{\alpha'}\rangle$ where α and α' stand for the modes of the two emitted quanta. Thus, these two states are written as $|i\rangle = |e; \text{vac}\rangle$ and as $|f\rangle = |g; 1_\alpha, 1_{\alpha'}\rangle$, respectively. In the intermediate states that connect these two states, the emitter is in an intermediate energy state $|m\rangle$ and the field is in a one-quantum state. Depending on which mode is the first emitted quantum, the intermediate states are written as $|l\rangle = |m; 1_\alpha\rangle$ or $|l\rangle = |m; 1_{\alpha'}\rangle$. Later, the energy of the emitter in the state $|a\rangle$ will be denoted as ε_a with $a = e, m, g$.

B. Interaction Hamiltonian

When the spatial variation of the electric field at the emitter's position is not negligible, which is possible when the photonic environment is a nanostructure supporting localized surface plasmons, the standard electric dipole approximation is no longer appropriate [10,27–30]. Therefore, we study the interaction Hamiltonian H_{int} of the system, which describes the emitter-field interactions, up to the electric quadrupolar order [6,51]:

$$H_{\text{int}}(\mathbf{R}, t) = \underbrace{-\mathbf{d} \cdot \mathbf{E}(\mathbf{R}, t)}_{H_{\text{ED}}} - \underbrace{\mathbf{m} \cdot \mathbf{B}(\mathbf{R}, t)}_{H_{\text{MD}}} - \underbrace{\mathbf{Q} : [\nabla \mathbf{E}(\mathbf{R}, t)]}_{H_{\text{EQ}}}, \quad (3)$$

in which the emitter's position \mathbf{R} is taken at the center of its charge distribution. In this equation, $\nabla = (\frac{\partial}{\partial x}, \frac{\partial}{\partial y}, \frac{\partial}{\partial z})^T$ is a column vector with T denoting the transpose, the dot product is the vector scalar product, the product $\nabla \mathbf{E}$ is an outer product, whereas the double dot product is defined as $\mathbf{T} : \mathbf{U} := \sum_{i,j} T_{...ij} U_{ji...}$ with \mathbf{T} and \mathbf{U} two tensors of rank greater than or equal to two. Moreover, \mathbf{d} , \mathbf{m} , and \mathbf{Q} are, respectively, the electric dipole (ED), the magnetic dipole (MD), and the electric quadrupole (EQ) moment operators.

Since a photon can be emitted by three different multipolar emission pathways (ED, MD, and EQ), there are nine possible contributions to the total TPSE rate. In this paper we focus on three contributions, namely, the two-electric dipole (2ED), two-magnetic dipole (2MD), and two-electric quadrupole (2EQ) second-order transitions, under which both photons are emitted by the same multipolar first-order transition. Other combinations can be derived with similar developments, but they are not relevant to the application we describe later on.

The electromagnetic field operators in Eq. (3) can be written as a function of the normal modes $\mathbf{A}_\alpha(\mathbf{r})$ of the vector potential [52,53]:

$$\mathbf{E}(\mathbf{r}, t) = i \sum_{\alpha} \sqrt{\frac{\hbar \omega_{\alpha}}{2 \varepsilon_0}} \{a_{\alpha}(t) \mathbf{A}_{\alpha}(\mathbf{r}) - a_{\alpha}^{\dagger}(t) \mathbf{A}_{\alpha}^*(\mathbf{r})\}, \quad (4a)$$

$$\mathbf{B}(\mathbf{r}, t) = \sum_{\alpha} \sqrt{\frac{\hbar}{2 \varepsilon_0 \omega_{\alpha}}} \{a_{\alpha}(t) \mathbf{B}_{\alpha}(\mathbf{r}) - a_{\alpha}^{\dagger}(t) \mathbf{B}_{\alpha}^*(\mathbf{r})\}, \quad (4b)$$

where $\mathbf{B}_{\alpha}(\mathbf{r}) := \nabla \times \mathbf{A}_{\alpha}(\mathbf{r})$ using the vector cross product. In these equations ε_0 is the vacuum electric permittivity, whereas $a_{\alpha}(t)$ and $a_{\alpha}^{\dagger}(t)$ are the annihilation and creation operators of a photon in the mode α of energy $\hbar \omega_{\alpha}$. Note that the modes $\mathbf{A}_{\alpha}(\mathbf{r})$ are normalized and form a complete set of solutions of the Helmholtz equation, subject to the boundary conditions imposed by the photonic environment. These are also the conditions applied to the modes that lead to the Purcell effect.

C. Multipolar emission channel contributions to the two-photon spontaneous emission rate

Since the states of the system and the interaction Hamiltonian are known, we can calculate each multipolar emission channel contribution to the two-photon transition rate using Eqs. (1) to (4). If the first-order Fermi's golden rule is used instead of the second-order one, we find the three multipolar emission channel contributions to the one-photon spontaneous emission rate [50]:

$$\Gamma_{\text{ED}}^{(1)}(\mathbf{R}) = \frac{\pi}{\varepsilon_0 \hbar} \sum_{\alpha} \omega_{\alpha} |\mathbf{d}^{eg} \cdot \mathbf{A}_{\alpha}|^2 \delta(\omega_{\text{eg}} - \omega_{\alpha}), \quad (5a)$$

$$\Gamma_{\text{MD}}^{(1)}(\mathbf{R}) = \frac{\pi}{\varepsilon_0 \hbar} \sum_{\alpha} \frac{1}{\omega_{\alpha}} |\mathbf{m}^{eg} \cdot [\nabla \times \mathbf{A}_{\alpha}]|^2 \delta(\omega_{\text{eg}} - \omega_{\alpha}), \quad (5b)$$

$$\Gamma_{\text{EQ}}^{(1)}(\mathbf{R}) = \frac{\pi}{\varepsilon_0 \hbar} \sum_{\alpha} \omega_{\alpha} |\mathbf{Q}^{eg} : [\nabla \mathbf{A}_{\alpha}]|^2 \delta(\omega_{\text{eg}} - \omega_{\alpha}), \quad (5c)$$

where the spatial dependency of the modes has been omitted. ω_{α} denotes the angular frequency of the photon in the mode α and $\hbar \omega_{\text{eg}} := \varepsilon_e - \varepsilon_g$ is the transition energy. Furthermore, $\mathbf{d}^{ab} := \langle a | \mathbf{d} | b \rangle$, $\mathbf{m}^{ab} := \langle a | \mathbf{m} | b \rangle$, and $\mathbf{Q}^{ab} := \langle a | \mathbf{Q} | b \rangle$ stand for the transition electric dipole, the transition magnetic dipole

and the transition electric quadrupole moments, respectively, which describe the emitter's transition from the state $|b\rangle$ to the state $|a\rangle$ ($a, b = e, m, g$). Notice that the electric dipole transition is due to the field modes evaluated at the center of charge of the emitter, while the magnetic dipolar and the electric quadrupolar ones are caused by the variation of the field modes.

Now we focus on the two-photon transition rates. One shows that the two-electric dipole contribution to the TPSE rate is given by [47,50]

$$\Gamma_{\text{2ED}}^{(2)}(\mathbf{R}) = \frac{\pi}{4 \varepsilon_0^2 \hbar^2} \sum_{\alpha, \alpha'} \omega_{\alpha} \omega_{\alpha'} |\mathbf{A}_{\alpha}(\mathbf{R}) \cdot \mathcal{D}^{eg} \cdot \mathbf{A}_{\alpha'}(\mathbf{R})|^2 \times \delta(\omega_{\text{eg}} - \omega_{\alpha} - \omega_{\alpha'}), \quad (6)$$

which involves a summation over the modes α and α' related to the two emitted quanta. In this equation we have defined the second-rank tensor

$$\mathcal{D}^{eg}(\omega_{\alpha}, \omega_{\alpha'}) := \sum_m \left(\frac{\mathbf{d}^{em} \mathbf{d}^{mg}}{\omega_{em} - \omega_{\alpha}} + \frac{\mathbf{d}^{mg} \mathbf{d}^{em}}{\omega_{em} - \omega_{\alpha'}} \right), \quad (7)$$

which depends on the frequencies of the two emitted quanta. The outer product is implied and $\hbar \omega_{ab} := \varepsilon_a - \varepsilon_b$. As this tensor involves two one-order transition electric dipole moments, the tensor \mathcal{D}^{eg} describes the two successive electric dipole transitions between the states $|e\rangle$ and $|g\rangle$ of the emitter. Subsequently, we refer to this tensor as the second-order transition electric dipole moment.

Following the same procedure we derive the two magnetic dipole (2MD) and the two electric quadrupole (2EQ) contributions to the TPSE rate (details relative to the 2EQ contribution in the Supplemental Material [49]):

$$\Gamma_{\text{2MD}}^{(2)}(\mathbf{R}) = \frac{\pi}{4 \varepsilon_0^2 \hbar^2} \sum_{\alpha, \alpha'} \frac{1}{\omega_{\alpha} \omega_{\alpha'}} |[\nabla \times \mathbf{A}_{\alpha}] \cdot \mathcal{M}^{eg} \cdot [\nabla \times \mathbf{A}_{\alpha'}]|^2 \times \delta(\omega_{\text{eg}} - \omega_{\alpha} - \omega_{\alpha'}), \quad (8a)$$

$$\Gamma_{\text{2EQ}}^{(2)}(\mathbf{R}) = \frac{\pi}{4 \varepsilon_0^2 \hbar^2} \sum_{\alpha, \alpha'} \omega_{\alpha} \omega_{\alpha'} |[\nabla \mathbf{A}_{\alpha}] : \mathcal{Q}^{eg} : [\nabla \mathbf{A}_{\alpha'}]|^2 \times \delta(\omega_{\text{eg}} - \omega_{\alpha} - \omega_{\alpha'}), \quad (8b)$$

In these expressions the spatial dependency of the field modes has been omitted, as well as the frequency dependence of the second-rank and fourth-rank tensors defined as

$$\mathcal{M}^{eg}(\omega_{\alpha}, \omega_{\alpha'}) := \sum_m \left(\frac{\mathbf{m}^{em} \mathbf{m}^{mg}}{\omega_{em} - \omega_{\alpha}} + \frac{\mathbf{m}^{mg} \mathbf{m}^{em}}{\omega_{em} - \omega_{\alpha'}} \right), \quad (9a)$$

$$\mathcal{Q}^{eg}(\omega_{\alpha}, \omega_{\alpha'}) := \sum_m \left(\frac{\mathbf{Q}^{em} \mathbf{Q}^{mg}}{\omega_{em} - \omega_{\alpha}} + \frac{\mathbf{Q}^{mg} \mathbf{Q}^{em}}{\omega_{em} - \omega_{\alpha'}} \right), \quad (9b)$$

where the outer product is implied. The components of the tensor that derive from the outer product of two tensors \mathbf{U} and \mathbf{V} are $(\mathbf{UV})_{i_1, i_2, \dots, i_n, j_1, j_2, \dots, j_n} := U_{i_1, i_2, \dots, i_n} V_{j_1, j_2, \dots, j_n}$. Thus, these tensors describe the two successive magnetic dipole and electric quadrupole transitions, respectively, between the states $|e\rangle$ and $|g\rangle$ of the emitter. Subsequently, we refer to them as the second-order transition magnetic dipole and electric quadrupole moments. Note that since \mathbf{Q} is symmetric, the fourth-rank tensor \mathcal{Q}^{eg} is also symmetric (i.e., $\forall i, j, k, l = 1, 2, 3, \mathcal{Q}_{ijkl}^{eg} = \mathcal{Q}_{jikl}^{eg}$ and $\mathcal{Q}_{ijlk}^{eg} = \mathcal{Q}_{ijlk}^{eg}$). Moreover,

since \mathbf{Q} can be taken traceless [54,55], with the definition of \mathcal{Q}^{eg} , the tensor satisfies the two following properties: $\forall k, l = 1, 2, 3, \sum_{i=1}^3 \mathcal{Q}_{ikl}^{eg} = 0$ and $\forall i, j = 1, 2, 3, \sum_{k=1}^3 \mathcal{Q}_{ijkk}^{eg} = 0$.

The derived equations (6) and (8) for the multipolar contributions to the TPSE rate are valid regardless of the emitter environment. We will now derive the rate of these transitions in vacuum. The obtained expressions will be useful in Sec. III to normalize transition rates, and to derive expressions for the multipolar contributions that can be computed through classical electromagnetic simulations.

D. Free-space two-photon spontaneous emission rate

In free space the field modes are plane waves defined by a wave vector \mathbf{k} and a unitary polarization vector $\mathbf{e}_{\mathbf{k},s}$ where the parameter $s = 1, 2$ represents the two transverse polarizations [50,52]. Consequently, the field modes in Eqs. (6) and (8) become

$$\mathbf{A}_\alpha(\mathbf{r}) \longrightarrow \mathbf{A}_{\mathbf{k},s}(\mathbf{r}) = \frac{e^{i\mathbf{k}\cdot\mathbf{r}}}{\sqrt{V}} \mathbf{e}_{\mathbf{k},s}, \quad (10)$$

where V stands for the arbitrary and finite-box quantization volume in which the field is assumed to be confined. In this case the summation over the modes α becomes [50,52]

$$\sum_\alpha \longrightarrow \sum_{s=1}^2 \sum_{\mathbf{k}} \xrightarrow{V \rightarrow \infty} \frac{V}{(2\pi)^3} \sum_{s=1}^2 \int d^3k. \quad (11)$$

The calculations for the 2ED transition can be found in Ref. [50], while the calculations relative to the 2EQ transition is in our Supplemental Material [49]. Thus, for each multipolar operator $\text{MO} \in \{\text{ED}, \text{MD}, \text{EQ}\}$ the free-space TPSE rate is given by

$$\Gamma_{2\text{MO},0}^{(2)} = \int_0^{\omega_{\text{eg}}} \gamma_{2\text{MO},0}^{(2)}(\omega) d\omega, \quad (12)$$

where each multipolar contribution $\gamma_{2\text{MO},0}^{(2)}(\omega)$ to the spectral distribution of the emitted quanta $\gamma_0^{(2)}(\omega)$ is given by

$$\gamma_{2\text{ED},0}^{(2)}(\omega) = \frac{\omega^3(\omega_{\text{eg}} - \omega)^3}{36\pi^3 \varepsilon_0^2 \hbar^2 c^6} \|\mathcal{D}^{eg}(\omega, \omega_{\text{eg}} - \omega)\|^2, \quad (13a)$$

$$\gamma_{2\text{MD},0}^{(2)}(\omega) = \frac{\omega^3(\omega_{\text{eg}} - \omega)^3}{36\pi^3 \varepsilon_0^2 \hbar^2 c^{10}} \|\mathcal{M}^{eg}(\omega, \omega_{\text{eg}} - \omega)\|^2, \quad (13b)$$

$$\gamma_{2\text{EQ},0}^{(2)}(\omega) = \frac{\omega^5(\omega_{\text{eg}} - \omega)^5}{400\pi^3 \varepsilon_0^2 \hbar^2 c^{10}} \|\mathcal{Q}^{eg}(\omega, \omega_{\text{eg}} - \omega)\|^2, \quad (13c)$$

where c denotes the speed of light in vacuum, and the squared norm of an n th-rank tensor \mathbf{U} with $n \in \mathbb{N}_0$ is $\|\mathbf{U}\|^2 := \sum_{i_1, i_2, \dots, i_n} |U_{i_1, i_2, \dots, i_n}|^2$.

III. RELATION BETWEEN THE TWO-PHOTON SPONTANEOUS EMISSION RATE AND PURCELL FACTORS

A connection between the TPSE rate of an emitter and the Purcell factors related to the one-photon spontaneous emission (OPSE) process was established for the 2ED transition [47]. However, this formula can only be used in the basis that

diagonalizes the imaginary part of the dyadic Green's function independently of the frequency, which is a condition that only allows the study of symmetric structures with emitters at specific positions. In further work, this formula was used to calculate TPSE spectra for the 2ED transition of a hydrogen-like emitter placed under a plasmonic two-dimensional silver nanodisk [48]. However, because of the aforementioned condition on the basis, they could only study the case where the emitter is on the axis of symmetry of the disk.

Consequently, it is interesting to take into account corrective terms, linked to the off-diagonal components of the imaginary part of the Green's function, in order to derive general formulas for the 2ED, 2MD, and 2EQ transition rates, which can be used for structures of arbitrary shape and at any emitter's position. Moreover, since the derived formulas are based on the calculation of Purcell factors, we emphasize here that the TPSE rate of an emitter can be determined through conventional classical electromagnetic simulations, thus allowing to consider arbitrary shaped nanostructures.

To this end we first normalize the multipolar contributions to the TPSE rate, Eqs. (6) and (8), with the free-space rates, and rewrite them as a function of the dyadic Green's function \mathbf{G} . Its imaginary part admits a spectral representation that can be expanded in terms of the normal modes \mathbf{A}_α of the electromagnetic field [6]

$$\text{Im}\mathbf{G}(\omega; \mathbf{r}, \mathbf{r}') = \frac{\pi c^2}{2\omega} \sum_\alpha \mathbf{A}_\alpha(\mathbf{r}) \mathbf{A}_\alpha^*(\mathbf{r}') \delta(\omega - \omega_\alpha). \quad (14)$$

Then, for each multipolar contribution we establish a connection between the Green's function and the one-photon Purcell factors. We start with the 2ED transition, next we extend this relation for the 2MD transition, and lastly for the 2EQ transition (detailed derivation in the Supplemental Material [49]).

A. Two-electric dipole transitions

By involving the Green's function and dividing the obtained spectral density $\gamma_{2\text{ED}}^{(2)}(\omega; \mathbf{R})$ by the free-space one [Eq. (13a)] we obtain [47]

$$\begin{aligned} \frac{\gamma_{2\text{ED}}^{(2)}(\omega; \mathbf{R})}{\gamma_{2\text{ED},0}^{(2)}(\omega)} &= \hat{\mathcal{D}}_{ia}^{eg}(\omega, \omega_{\text{eg}} - \omega) [\hat{\mathcal{D}}_{jb}^{eg}(\omega, \omega_{\text{eg}} - \omega)]^* \\ &\times \frac{6\pi c}{\omega} \text{Im}G_{ij}(\omega; \mathbf{R}, \mathbf{R}) \\ &\times \frac{6\pi c}{\omega_{\text{eg}} - \omega} \text{Im}G_{ab}(\omega_{\text{eg}} - \omega; \mathbf{R}, \mathbf{R}), \end{aligned} \quad (15)$$

where the Einstein summation convention is used and the caret denotes normalized tensors (i.e., for an n th-rank tensor \mathbf{U} with $n \in \mathbb{N}_0$, $\hat{\mathbf{U}} := \mathbf{U}/\|\mathbf{U}\|$). Note that the indices i and j are related to the quantum emitted at the frequency ω while the indices a and b concern the quantum emitted at the complementary frequency $\omega_{\text{eg}} - \omega$.

1. Relation with the Purcell factors

To establish the relation between the components of the Green's function and the one-photon Purcell factors, let us

consider the ED transition rate written as [6]

$$\frac{\Gamma_{\text{ED}}^{(1)}(\mathbf{R})}{\Gamma_{\text{ED},0}^{(1)}} = \hat{d}_i^{eg} (\hat{d}_j^{eg})^* \frac{6\pi c}{\omega_{\text{eg}}} \text{Im} G_{ij}(\omega_{\text{eg}}; \mathbf{R}, \mathbf{R}), \quad (16)$$

where $\hat{\mathbf{d}}^{eg}$ stands for the normalized one-order transition electric dipole moment.

A general electric dipole moment can be expanded with an orthonormal basis of three dipoles. We define the Purcell factors P_i^{ED} , which correspond to the ratio between the ED transition rate of an emitter that has its transition electric dipole moment aligned along one of the basis vectors (i.e., $\hat{\mathbf{d}}^{eg} := \hat{\mathbf{e}}_i$ with $i = 1, 2, 3$) and the corresponding rate in free space as [47]

$$P_i^{\text{ED}}(\omega; \mathbf{R}) := \frac{6\pi c}{\omega} \text{Im} G_{ii}(\omega; \mathbf{R}, \mathbf{R}). \quad (17)$$

Furthermore, we define the Purcell factors P_{ij}^{ED} relative to an emitter that has its transition electric dipole moment aligned along the bisector of two basis vectors [i.e., $\hat{\mathbf{d}}^{eg} := (\hat{\mathbf{e}}_i + \hat{\mathbf{e}}_j)/\sqrt{2}$ with $i, j = 1, 2, 3$ and $i \neq j$] as

$$P_{ij}^{\text{ED}}(\omega; \mathbf{R}) := \frac{1}{2} [P_i^{\text{ED}}(\omega; \mathbf{R}) + P_j^{\text{ED}}(\omega; \mathbf{R})] + \frac{6\pi c}{\omega} \text{Im} G_{ij}(\omega; \mathbf{R}, \mathbf{R}), \quad (18)$$

where we used the definition of the Purcell factors P_i^{ED} as well as the symmetry property of the tensor $\text{Im} \mathbf{G}$ [56].

We can now rewrite equation (15) as

$$\frac{\gamma_{2\text{ED}}^{(2)}(\omega; \mathbf{R})}{\gamma_{2\text{ED},0}^{(2)}(\omega)} = \hat{D}_{ia}^{eg}(\omega, \omega_{\text{eg}} - \omega) [\hat{D}_{jb}^{eg}(\omega, \omega_{\text{eg}} - \omega)]^* \times F_{ij}^{\text{ED}}(\omega; \mathbf{R}) F_{ab}^{\text{ED}}(\omega_{\text{eg}} - \omega; \mathbf{R}), \quad (19)$$

where the components of the tensor \mathbf{F}^{ED} are defined as

$$F_{ii}^{\text{ED}}(\omega; \mathbf{R}) := \frac{6\pi c}{\omega} \text{Im} G_{ii}(\omega; \mathbf{R}, \mathbf{R}) = P_i^{\text{ED}}(\omega; \mathbf{R}), \quad (20)$$

$$F_{ij}^{\text{ED}}(\omega; \mathbf{R}) := \frac{6\pi c}{\omega} \text{Im} G_{ij}(\omega; \mathbf{R}, \mathbf{R}) = P_{ij}^{\text{ED}}(\omega; \mathbf{R}) - \frac{1}{2} [P_i^{\text{ED}}(\omega; \mathbf{R}) + P_j^{\text{ED}}(\omega; \mathbf{R})], \quad (21)$$

with $i, j = 1, 2, 3$ and $i \neq j$. Note that we can also rewrite equation (16) of the ED transition rate as a function of this tensor.

Since this tensor \mathbf{F}^{ED} is also symmetric we need to calculate in the most general case six Purcell factors to get the 2ED transition rate. For example, in a Cartesian basis we need to calculate these six factors:

$$\{P_x^{\text{ED}}, P_y^{\text{ED}}, P_z^{\text{ED}}, P_{yz}^{\text{ED}}, P_{xz}^{\text{ED}}, P_{xy}^{\text{ED}}\}. \quad (22)$$

In free-space all Purcell factors are equal to one and so the tensor \mathbf{F}^{ED} is equal to the identity matrix.

As a consistency check, in the basis that diagonalizes the imaginary part of the Green's function simultaneously at the frequencies of the two emitted quanta (or in the range of the studied spectrum), we retrieve the less general formula (valid

only in this specific basis) that involves only the three Purcell factors P_i^{ED} [47]:

$$\frac{\gamma_{2\text{ED}}^{(2)}(\omega; \mathbf{R})}{\gamma_{2\text{ED},0}^{(2)}(\omega)} = |\hat{D}_{ia}^{eg}(\omega, \omega_{\text{eg}} - \omega)|^2 \times P_i^{\text{ED}}(\omega; \mathbf{R}) P_a^{\text{ED}}(\omega_{\text{eg}} - \omega; \mathbf{R}). \quad (23)$$

B. Two-magnetic dipole transition

Similar developments lead to the 2MD transition rate:

$$\frac{\gamma_{2\text{MD}}^{(2)}(\omega; \mathbf{R})}{\gamma_{2\text{ED},0}^{(2)}(\omega)} = \hat{\mathcal{M}}_{ia}^{eg}(\omega, \omega_{\text{eg}} - \omega) [\hat{\mathcal{M}}_{jb}^{eg}(\omega, \omega_{\text{eg}} - \omega)]^* \times F_{ij}^{\text{MD}}(\omega; \mathbf{R}) F_{ab}^{\text{MD}}(\omega_{\text{eg}} - \omega; \mathbf{R}), \quad (24)$$

involving the normalized second-order transition magnetic dipole moment, as well as the tensor \mathbf{F}^{MD} . Equations (20) and (21) that establish the link between the tensor \mathbf{F}^{ED} and the Purcell factors for the ED transition are also valid for the MD transition, where the Purcell factors are defined in the same way, but with the transition magnetic dipole moment instead.

C. Two-electric quadrupole transition

Let us now focus on the 2EQ transition. Via the Green's function [Eq. (14)] and dividing the obtained spectral density $\gamma_{2\text{EQ}}^{(2)}(\omega; \mathbf{R})$ by the free-space one [Eq. (13c)] we get [49]

$$\frac{\gamma_{2\text{EQ}}^{(2)}(\omega; \mathbf{R})}{\gamma_{2\text{EQ},0}^{(2)}(\omega)} = \hat{Q}_{ijab}^{eg}(\omega, \omega_{\text{eg}} - \omega) [\hat{Q}_{klcd}^{eg}(\omega, \omega_{\text{eg}} - \omega)]^* \times T_{ijkl}(\omega; \mathbf{R}) T_{abcd}(\omega_{\text{eg}} - \omega; \mathbf{R}), \quad (25)$$

where the Einstein summation convention is used and \hat{Q}^{eg} stands for the normalized second-order transition electric quadrupole moment. Note that the indices i, j, k , and l are related to the quanta emitted at the frequency ω , while the indices a, b, c , and d concern the quanta emitted at the complementary frequency $\omega_{\text{eg}} - \omega$.

In the previous equation we use the fourth-rank tensor \mathbf{T} defined as

$$T_{ijkl}(\omega; \mathbf{R}) := \frac{20\pi c^3}{\omega^3} \{\partial_j \partial_{l'} \text{Im} G_{ik}(\omega; \mathbf{r}, \mathbf{r}')\}_{\mathbf{r}=\mathbf{r}'=\mathbf{R}}, \quad (26)$$

where ∂_j and $\partial_{l'}$ mean derivatives with respect to, respectively, the coordinates \mathbf{r} and \mathbf{r}' . Since \mathbf{T} is a real tensor, by using Eq. (14) we can show that it satisfies the property $\forall i, j, k, l = 1, 2, 3, T_{ijkl} = T_{klij}$.

The derived equation contains 9^4 terms. Fortunately, we can use the property of the tensor \mathbf{T} mentioned above, as well as the properties of the tensor \hat{Q}^{eg} derived from the symmetric and traceless properties of electric quadrupole moments (cf. Sec. II C), to remove redundant components. We obtain a formula involving only $(\sum_{n=1}^5 n)^2 = 15^2$ terms [49]:

$$\frac{\gamma_{2\text{EQ}}^{(2)}(\omega; \mathbf{R})}{\gamma_{2\text{EQ},0}^{(2)}(\omega)} = \sum_{\substack{\mu, \nu=1 \\ \nu \geq \mu}}^5 \sum_{\substack{\alpha, \beta=1 \\ \beta \geq \alpha}}^5 \hat{Q}_{\mu\alpha\nu\beta}^{eg}(\omega, \omega_{\text{eg}} - \omega) \times F_{\mu\nu}^{\text{EQ}}(\omega; \mathbf{R}) F_{\alpha\beta}^{\text{EQ}}(\omega_{\text{eg}} - \omega; \mathbf{R}), \quad (27)$$

TABLE I. Modified Voigt notation: correspondence between the pair of indices (i, j) of a symmetric and traceless tensor in three dimensions and the indices μ in five dimensions. The indices $\mu = 1, 2$ correspond to the two independent diagonal components of a second-rank tensor, while the indices $\mu = 3, 4, 5$ correspond to its three independent off-diagonal components. By convention, the indices of this notation are denoted with Greek letters.

(i, j)	(1,1)	(2,2)	(2,3)	(1,3)	(1,2)
μ	1	2	3	4	5

where the indices μ and ν are relative to the first quantum, while the indices α and β are relative to the second one. In this equation the second-rank tensor \mathbf{F}^{EQ} in five dimensions is expressed as a function of the tensor \mathbf{T} [49], and the components of the fourth-rank tensor $\hat{\mathbf{Q}}^{\text{eg}}$ in five dimensions is defined as

$$\hat{Q}_{\mu\alpha\nu\beta} := \begin{cases} \hat{Q}_{\mu\alpha} \hat{Q}_{\nu\beta}^* & \forall \mu = \nu, \quad \alpha = \beta \\ \hat{Q}_{\mu\alpha} \hat{Q}_{\nu\beta}^* + \hat{Q}_{\mu\beta} \hat{Q}_{\nu\alpha}^* & \forall \mu = \nu, \quad \alpha < \beta \\ \hat{Q}_{\mu\alpha} \hat{Q}_{\nu\beta}^* + \hat{Q}_{\nu\alpha} \hat{Q}_{\mu\beta}^* & \forall \mu < \nu, \quad \alpha = \beta \\ 2\hat{Q}_{\mu\alpha} \hat{Q}_{\nu\beta}^* + 2\hat{Q}_{\mu\beta} \hat{Q}_{\nu\alpha}^* & \forall \mu < \nu, \quad \alpha < \beta, \end{cases} \quad (28)$$

where the *eg* superscript and the dependencies are omitted.

To derive this formula we use a modified version of the Voigt notation. This mathematical convention exploits the symmetry and the traceless properties of a tensor by removing its redundant components to represent it by a lower-rank tensor defined in a higher-dimensional space. In this way the one-order and two-order transition electric quadrupole moments, which are second-rank and fourth-rank tensors in three dimensions, are represented by means of a vector and a second-rank tensor in five dimensions, respectively. Table I establishes the correspondence between the new indices and these of the represented tensors.

1. Relation with Purcell factors

As for the 2ED transition we first consider the one-photon EQ transition rate in order to establish the relation between the tensor \mathbf{F}^{EQ} and the one-photon Purcell factors, which are defined here as the ratio between the one-photon EQ transition rate and the corresponding rate in free space.

We can show that the EQ transition can be written as [49]

$$\frac{\Gamma_{\text{EQ}}^{(1)}(\mathbf{R})}{\Gamma_{\text{EQ},0}^{(1)}} = \sum_{\substack{\mu, \nu=1 \\ \nu \geq \mu}}^5 \hat{Q}_{\mu\nu}^{\text{eg}} F_{\mu\nu}^{\text{EQ}}(\omega_{\text{eg}}; \mathbf{R}), \quad (29)$$

with the second-rank tensor $\hat{\mathbf{Q}}^{\text{eg}}$ in five dimensions defined as

$$\hat{Q}_{\mu\nu}^{\text{eg}} := \begin{cases} \hat{Q}_{\mu}^{\text{eg}} (\hat{Q}_{\mu}^{\text{eg}})^* & \forall \mu = \nu \\ 2\hat{Q}_{\mu}^{\text{eg}} (\hat{Q}_{\nu}^{\text{eg}})^* & \forall \mu < \nu. \end{cases} \quad (30)$$

Since a general electric quadrupole moment involves up to five independent components, it can be expanded with a basis of five quadrupoles. To construct this basis we consider two different types of quadrupole, sketched in Fig. 1. In our notation these quadrupoles are represented by a vector in five

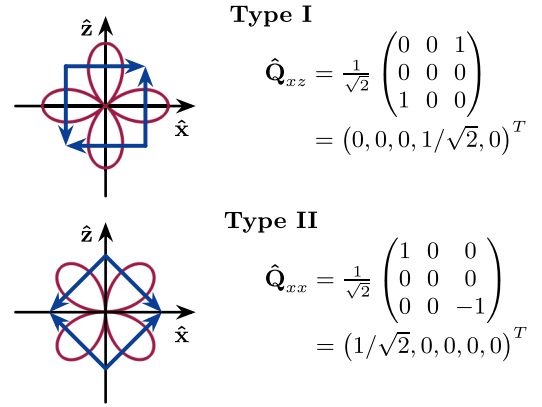


FIG. 1. Representation of the two considered types of plane quadrupole configurations. Type II differs from type I by a rotation of 45° in the plane and involves only diagonal components, while type I involves solely off-diagonal components. They are represented by means of four dipoles of same norm (blue arrows) and the radiation patterns are sketched in dark red. The modified Voigt notation is used to represent their tensor by the means of a five-dimensional vector.

dimensions where only the μ th component is nonzero and equals $1/\sqrt{2}$.

First, we define five Purcell factors P_{μ}^{EQ} where the indices $\{\mu = 1, \dots, 5\}$ correspond, respectively, to the indices $\{xx, yy, yz, xz, xy\}$ (three types I and two types II):¹

$$P_{\mu}^{\text{EQ}}(\omega; \mathbf{R}) := \frac{1}{2} F_{\mu\mu}^{\text{EQ}}(\omega; \mathbf{R}) \quad \forall \mu = 1, \dots, 5. \quad (31)$$

These factors correspond to the ratio between the EQ transition rate of an emitter for which its transition electric quadrupole moment is the basis tensor $\hat{\mathbf{Q}}_{\mu}$ and the corresponding rate in free space.

Second, we consider all of the possible combinations of the basis quadrupoles:²

$$\hat{\mathbf{Q}}_{\mu\nu} := \frac{1}{N} (\hat{\mathbf{Q}}_{\mu} + \hat{\mathbf{Q}}_{\nu}) \quad \forall \mu, \nu = 1, \dots, 5, \quad \mu < \nu, \quad (32)$$

with N a normalization constant. This allows us to define ten Purcell factors:

$$P_{\mu\nu}^{\text{EQ}} := \begin{cases} \frac{1}{3} (P_{\mu} + P_{\nu} + F_{\mu\nu}) & \text{if } (\mu, \nu) = (1, 2) \\ \frac{1}{2} (P_{\mu} + P_{\nu} + F_{\mu\nu}) & \forall \mu, \nu = 2, 3, 4, 5, \quad \mu < \nu, \end{cases} \quad (33)$$

where the EQ superscript and the dependencies have been omitted and where the Purcell factors $P_{\mu\nu}^{\text{EQ}}$ are relative to an emitter that has its transition electric quadrupole moment described by the tensor $\hat{\mathbf{Q}}_{\mu\nu}$ (i.e., an equal and linear combination of the tensors $\hat{\mathbf{Q}}_{\mu}$ and $\hat{\mathbf{Q}}_{\nu}$).

To summarize, we established a relation between the 15 independent components of the symmetric tensor \mathbf{F}^{EQ} , which

¹We do not need to consider the type-II quadrupole $\hat{\mathbf{Q}}_{zz}$ because, in our modified Voigt notation, we removed the last diagonal component to remove redundancy with respect to the traceless property.

²Note that all considered quadrupoles need to be normalized and that the quadrupole $\hat{\mathbf{Q}}_{xxyy} = (\hat{\mathbf{Q}}_{xx} + \hat{\mathbf{Q}}_{yy})/\sqrt{3}$ is the linear quadrupole represented by the diagonal matrix $1/\sqrt{6} \text{diag}(1, 1, -2)$.

are related to the derivatives of the imaginary part of the dyadic Green's function, and 15 Purcell factors:

$$F_{\mu\nu}^{\text{EQ}}(\omega; \mathbf{R}) = \begin{cases} 2P_{\mu}^{\text{EQ}} & \forall \mu = \nu \\ 3P_{\mu\nu}^{\text{EQ}} - P_{\mu}^{\text{EQ}} - P_{\nu}^{\text{EQ}} & \text{if } (\mu, \nu) = (1, 2) \\ 2P_{\mu\nu}^{\text{EQ}} - P_{\mu}^{\text{EQ}} - P_{\nu}^{\text{EQ}} & \text{else,} \end{cases} \quad (34)$$

where the dependencies have been omitted. Thus, in the most general case these 15 Purcell factors are necessary to calculate the 2EQ transition rate:

$$\{P_{\mu}^{\text{EQ}}\} \cup \{P_{\mu\nu}^{\text{EQ}}\}, \quad (35)$$

where the indices $\mu, \nu = 1, \dots, 5$ with $\mu < \nu$ correspond to the indices $\{xx, yy, yz, xz, xy\}$. In vacuum all Purcell factors tend towards one and so \mathbf{F}^{EQ} is given by

$$F_{\mu\nu}^{\text{EQ}} = \begin{cases} 2 & \forall \mu = \nu \\ 1 & \text{if } (\mu, \nu) = (1, 2) \\ 0 & \text{else.} \end{cases} \quad (36)$$

D. Discussion

It is important to note that the derived equations for the multipolar contributions to the total TPSE rate [Eqs. (19), (24), and (27)] are valid regardless of the emitter environment. It is thus possible to calculate the change in spontaneous emission rates when the emitter is placed in a given photonic environment. Moreover, the contribution of the electronic structure of the emitter and the contribution of the photonic environment are decoupled in these equations, and thus can be calculated separately. Indeed, each equation involves two tensors. The first one is the normalized multipolar second-order transition moment that depends only on the electronic structure. The second one is the tensor \mathbf{F}^{MO} , with $\text{MO} \in \{\text{ED}, \text{MD}, \text{EQ}\}$, presents for the two emitted quanta of complementary energy and that is expressed as a function of the one-photon Purcell factors, and thus it depends only on the photonic environment.

It is known that the Purcell factors can be computed classically by the ratio of the power emitted by a classical emitter (i.e., a radiating point ED, MD, or EQ) in presence of the photonic environment and in free-space $P^{\text{MO}}(\omega; \mathbf{R}) = W_{\text{MO}}(\omega; \mathbf{R})/W_{\text{MO},0}(\omega)$ [6]. Furthermore, there is a dependency on the emitter's orientation with respect to the photonic environment. In the end these Purcell factors can be computed by modeling point sources in conventional electromagnetic software packages (with e.g., the finite-element method [57], the finite-difference time-domain method [58], etc.). The expression of the free-space emitted power for point sources can be found in Ref. [54].

In an emission process a quantum can be emitted either radiatively in case of photon emission to the far field, or nonradiatively in case of energy absorption by the environment. Since our framework is based on Purcell factors we can separate the contributions of the radiative and nonradiative emission channels to the TPSE process [48]. They can be calculated through the decomposition into radiative and nonradiative parts of the total Purcell factors: $P^{\text{MO}}(\omega, \mathbf{r}) = P_{\text{r}}^{\text{MO}}(\omega, \mathbf{r}) + P_{\text{nr}}^{\text{MO}}(\omega, \mathbf{r})$ [6,48].

Furthermore, as the TPSE process is continuous [59], retrieving a full TPSE spectrum requires the calculation of the

Purcell factors over a range of frequencies. In addition, at each frequency the Purcell factors need to be calculated for different source orientations. In the most general case, six Purcell factors are needed for the dipolar transitions [cf. Eq. (22)], while for the quadrupolar one 15 are needed [cf. Eq. (35)]. However, depending on the symmetry of the studied photonic environment some factors can be equal, thus reducing the number of Purcell factors to calculate.

Once the one-photon Purcell factors are calculated classically, one can straightforwardly determine each multipolar contribution to the TPSE rate via equations (19), (24), and (27) when the normalized multipolar second-order transition moments are known. In our framework these are calculated analytically via the wave functions of the emitter.

IV. APPLICATION

As a validation step of the developed framework, we study the two-photon Purcell effect for an $s \rightarrow s$ transition of a hydrogen atom placed 10 nm under a quasi-two-dimensional silver nanodisk, with the same system's parameters as in Ref. [48]. In this study, they calculated the 2ED contribution to the TPSE rate in the specific case where the emitter is placed on the axis of symmetry of the disk and with an analytical calculation of Purcell factors [48]. With our more general framework, the Purcell factors are computed numerically and the 2EQ contribution is also determined. Subsequently, we exploit the flexibility of our method in the case of an off-axis emitter. Note that since the considered structure is not relevant to enhance MD transitions [22], we did not calculate the magnetic contributions to the TPSE rate. Furthermore, the mixed ED-EQ two-photon $s \rightarrow s$ transition is not allowed by selection rules [35,60]. Our methods are explained below and then the results are presented and discussed.

A. Methods

Concerning the analytical calculation of the second-order transition moments, the determination of the tensor \mathcal{D}^{eg} can be found in Ref. [47] while the derivation of \mathcal{Q}^{eg} is given in our Supplemental Material [49]. The obtained tensors are independent of the frequencies of the emitted quanta and are respectively given by

$$\hat{\mathcal{D}}^{eg} = \frac{\mathbb{1}_3}{\sqrt{3}}, \quad (37a)$$

$$\hat{\mathcal{Q}}^{eg} = \frac{1}{\sqrt{20}} \begin{pmatrix} 4/3 & -2/3 & 0 & 0 & 0 \\ -2/3 & 4/3 & 0 & 0 & 0 \\ 0 & 0 & 1 & 0 & 0 \\ 0 & 0 & 0 & 1 & 0 \\ 0 & 0 & 0 & 0 & 1 \end{pmatrix}, \quad (37b)$$

where $\mathbb{1}_3$ is the identity matrix in three dimensions.

Near a low-loss plasmonic structure the nonradiative emission channel is dominated by the excitation of dark plasmonic modes, leading to absorption and no emission in the far field [48]. Thus, the two-quanta spontaneous emission process of an emitter close to this type of structure is dominated by

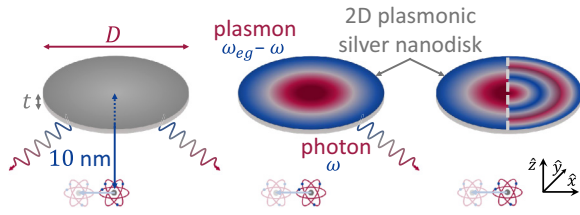


FIG. 2. From left to right: photon-photon, photon-plasmon, and plasmon-plasmon emission channels of the TPSE rate between two symmetric states of a quantum emitter. The latter is placed on-axis or off-axis 10 nm below a 5.2 Å thickness silver disk and its transition frequency is $\hbar\omega_{eg} = 2.64$ eV, which corresponds to a wavelength of 470 nm. The first quantum is emitted at the frequency ω while the second one is emitted at the complementary frequency $\omega_{eg} - \omega$.

three emission pathways, namely the photon-photon, photon-plasmon, and plasmon-plasmon channels (Fig. 2), which can be computed through the decomposition of the Purcell factors into radiative and nonradiative parts.

When the emitter is on-axis the system has azimuthal symmetry, reducing the number of Purcell factors to calculate. Thus, at each frequency three Purcell factors for the dipolar transition and seven for the quadrupolar one need to be calculated: $\{P_x^{ED}, P_z^{ED}, P_{xz}^{ED}\}$ and $\{P_{xx}^{EQ}, P_{xz}^{EQ}, P_{xy}^{EQ}, P_{xxyy}^{EQ}, P_{xxzz}^{EQ}, P_{xxyy}^{EQ}, P_{xzyy}^{EQ}\}$, where the Z

direction has been taken perpendicular to the disk. In contrast, when the emitter is shifted in the X direction, the system has no longer an azimuthal symmetry but rather a XZ -plane mirror symmetry and all factors (6 + 15) need to be calculated [cf. Eqs. (22) and (35)].

In practice each Purcell factor is computed over a range of frequencies with the COMSOL MULTIPHYSICS® software, which is based on the finite-element method, on a single core of a computer using an AMD Ryzen Threadripper PRO 5995WX CPU and 256 GB of RAM, thus enabling parallel computation. The parameters of our comsol models in the frequency domain are the following. First, the domain is a sphere with a radius equal to the studied wavelength λ and an unstructured tetrahedral mesh is used where the smallest element has a characteristic size of 0.25 nm. Second, perfectly matched layers (PMLs) are defined as an outer layer of the domain with a thickness of $\lambda/4$. Third, the silver nanodisk is modeled using a cylinder with a height $t = 5.2$ Å and a diameter $D = 25$ or 60 nm. Its optical response is given by the Drude conductivity $\sigma(\omega) = \epsilon_0\tau\omega_p^2/(1 - i\omega\tau)$ with the plasma frequency $\hbar\omega_p = 9.1$ eV and the relaxation rate of silver $\hbar\tau^{-1} = 18$ meV, as used in Ref. [48]. Fourth, the classical emitter is placed 10 nm under the nanodisk and is modeled by a radiating electric point dipole or quadrupole. Fifth, the Purcell factors are calculated by integration of the emitted power either at the inner surface of the PML for the radiative part or

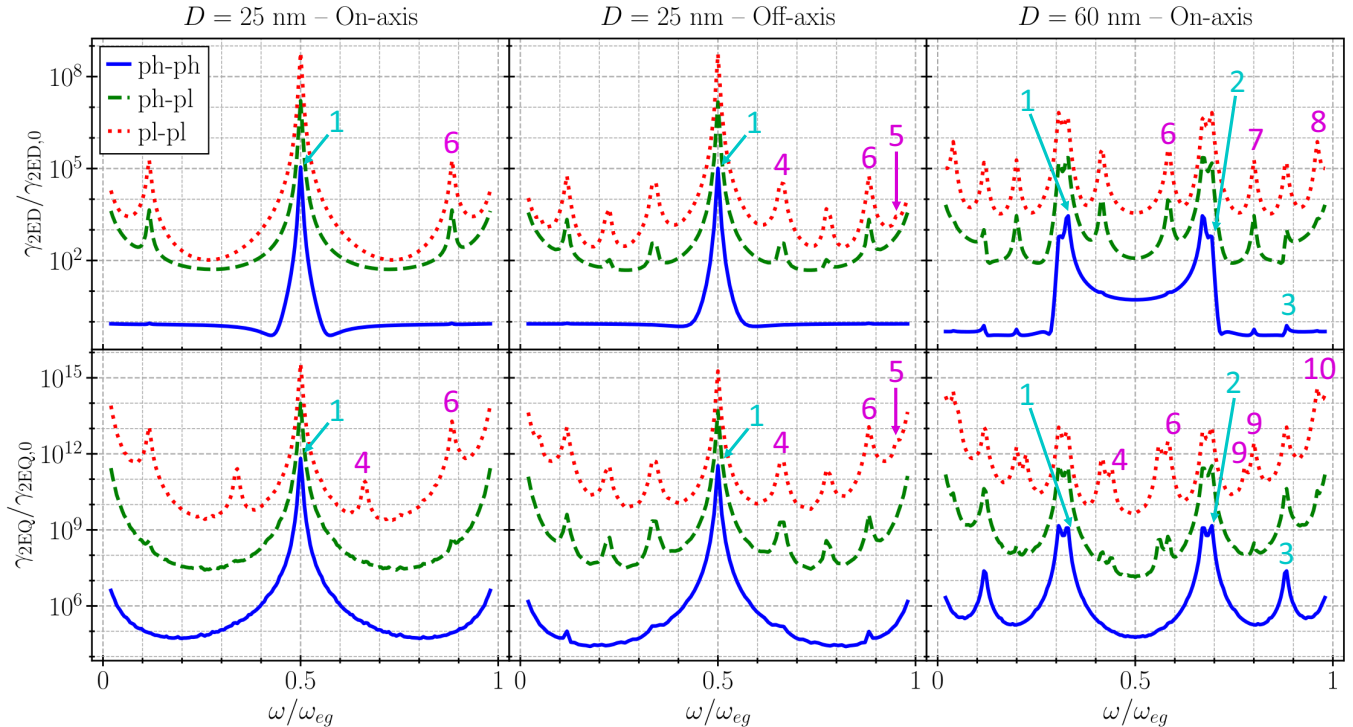


FIG. 3. Photon-photon (ph-ph), photon-plasmon (ph-pl), and plasmon-plasmon (pl-pl) relaxation channels of the spectral TPSE rate for the 2ED (top row) and 2EQ (bottom row) transitions between two symmetric states of a quantum emitter. The latter is placed 10 nm below a 5.2 Å thickness silver disk and its transition frequency is $\hbar\omega_{eg} = 2.64$ eV. The first two columns correspond to a 25 nm diameter disk, while for the third one the diameter is 60 nm. The emitter is placed on the axis of symmetry of the disk, except for the central column where it is shifted in the direction parallel to the disk by $D/4$. The spectra were computed over 199 frequencies for the emitter on-axis and over 99 frequencies for the emitter off-axis. The first quantum is emitted at the frequency ω while the second one is emitted at the complementary frequency $\omega_{eg} - \omega$, leading to symmetric spectra. In Fig. 4, the surface current density on the disk corresponding to some radiative and nonradiative peaks, which are identified by respectively a cyan and magenta number, is plotted.

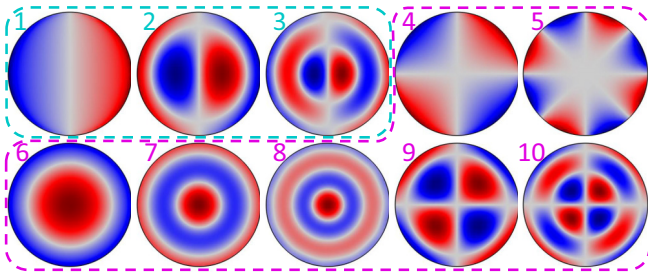


FIG. 4. Surface current density on the silver nanodisk relative to some radiative and nonradiative peaks, which are numbered respectively in cyan and magenta in Fig. 3. These plots were obtained by the excitation of the modes on the structure with a specific orientation of the emitter, either a dipole or a quadrupole. For example, the mode 1 can be obtained with a dipole oriented along the X axis but also with the quadrupole \hat{Q}_{xz} , while the mode 10 can only be obtained with quadrupoles, with for example \hat{Q}_{xx} and \hat{Q}_{xy} .

at the surface of a fictional sphere of 5 nm radius centered on the emitter for the total part (radiative plus nonradiative).

B. Results

The photon-photon, photon-plasmon, and plasmon-plasmon relaxation channels of the spectral TPSE rate for the 2ED and 2EQ contributions are plotted in Fig. 3. The emitter is placed on-axis for the spectra in the first and in the last columns, while it is shifted by a quantity $D/4$ in the plane parallel to the disk for the spectra in the central column. The computation of one Purcell factor over 199 frequencies has required 45 minutes and 13 GB of RAM for the 25 nm diameter disk, and 135 minutes and 30 GB of RAM for the 60 nm diameter one.

First of all, our results obtained for the ED two-quanta transition where the emitter is placed on-axis (top left and top right spectra) correspond to the results in Ref. [48] with their analytical calculation of Purcell factors with a plasmon wave-function formalism, thus confirming our method. Furthermore, the 2ED and 2EQ transitions are strongly enhanced by the plasmonic disk. Indeed, with the 25 nm diameter disk (left spectra) at $\omega = \omega_{eg}/2$, i.e., the frequency where both photons have the same energy, the 2ED and 2EQ transition rates are enhanced by, respectively, 8 and 15 orders of magnitude for the emission of two plasmons (dotted red line) and by, respectively, a factor $1.12 \times 10^5 (\pm 0.4\%)$ and $7.5 \times 10^{11} (\pm 5\%)$ for the emission of two photons (solid blue line). The standard deviation, expressed in percent, has been calculated by computing the COMSOL models at this frequency with finer mesh parameters.

Concerning the comparison of the different spectra, the surface current density of some modes excited on the disk is plotted in Fig. 4. We first observe that the 2EQ spectrum relative to a 25 nm diameter disk (bottom left spectrum) has an additional nonradiative peak compared with the 2ED one (top left spectrum) that corresponds to a quadrupolar mode (cf. mode number 4 in Fig. 4). Second, when the emitter is shifted (central spectra), the breaking of the azimuthal symmetry of the system leads to a greater wealth of excited modes (cf.

nonradiative mode numbers 4 and 5 in Fig. 4, note that the mode 5 peak is weakly visible at the scale of the figure), but the central radiative peak is slightly reduced. Note that in the off-axis configuration (central spectra), the 2ED spectra (top central spectrum) exhibits a peak (mode 4) corresponding to a quadrupolar mode excited on the structure, which was not possible to excite in the more symmetric on-axis configuration (top left spectrum). Third, when the diameter of the disk increases (right spectra), the frequency of the peaks changes and new, both radiative and nonradiative, peaks appear, which correspond to higher-order modes (cf. mode numbers 2, 3, 7, 8, 9, and 10 in Fig. 4). Remark, for example, that the dipolar mode 1 appears multiple times, such as in Fig. 3 top left and top right. The modes at these peaks have the same shape (Fig. 4), but there is a frequency shift because of the different disk radius. Note that only the bright peaks would show up in scattering spectra [61–63].

V. CONCLUSION

We develop a general framework to efficiently calculate two-photon spontaneous emission spectra of a quantum emitter in the vicinity of an arbitrary shaped nanostructure. It is based on the analytical calculation of the emitter contribution and, for the environment, on the classical computation of Purcell factors related to one-photon spontaneous emission. The latter are calculated by modeling classical point emitters in electromagnetic simulations, thus facilitating more complex geometries without available analytical models. Moreover, our framework goes beyond the dipolar approximation by taking into account the second-order multipolar interactions and is therefore relevant for plasmonic nano- and picocavities in which light is highly confined. In addition, our framework allows us to calculate separately the radiative and nonradiative emission channels, which is important to distinguish for many applications.

As a direct application we use the COMSOL MULTIPHYSICS® software to show an enhancement of 5 and 11 orders of magnitude for the electric dipole and quadrupole two-photon transitions for the $s \rightarrow s$ transition of a hydrogen-like emitter placed under a plasmonic silver nanodisk. Subsequently, the flexibility of our framework allows the optimization and the design of platforms for efficient entangled two-photon sources as an alternative to the conventional parametric down-conversion sources. These devices can include periodic structures in order to enhance the photon pair emission rate in the far field [64]. For on-chip sources one proposes nanostructures joined to waveguides [65], photonic crystals [66], or cavities [67] in order to create an integrated two-photon source. The method can be used to study two-photon spontaneous process for diverse quantum emitters and can be extended for example by including interference between the multipolar emission channels of this process [28].

ACKNOWLEDGMENTS

We acknowledge support from the FRS-FNRS (Research project T.0166.20) and from Action de Recherche Concertée (Project No. ARC-21/25 UMONS2).

- [1] P. Dirac, The quantum theory of the emission and absorption of radiation, *Proc. R. Soc. London, Ser. A* **114**, 243 (1927).
- [2] C. Cohen-Tannoudji, J. Dupont-Roc, and G. Grynberg, *Atom-Photon Interactions: Basic Process and Applications*, 1st ed. (Wiley-VCH Verlag GmbH & Co. KGaA, Weinheim, 1998).
- [3] P. W. Milonni, Why spontaneous emission? *Am. J. Phys.* **52**, 340 (1984).
- [4] W. Demtröder, *Atoms, Molecules and Photons*, Graduate Texts in Physics (Springer, Berlin, Heidelberg, 2010).
- [5] E. M. Purcell, H. C. Torrey, and R. V. Pound, Resonance absorption by nuclear magnetic moments in a solid, *Phys. Rev.* **69**, 37 (1946).
- [6] L. Novotny and B. Hecht, *Principles of Nano-Optics*, 2nd ed. (Cambridge University Press, Cambridge, 2012).
- [7] M. Thomas, J.-J. Greffet, R. Carminati, and J. R. Arias-Gonzalez, Single-molecule spontaneous emission close to absorbing nanostructures, *Appl. Phys. Lett.* **85**, 3863 (2004).
- [8] M. Born and E. Wolf, *Principles of Optics: Electromagnetic Theory of Propagation, Interference and Diffraction of Light*, 7th ed. (Cambridge University Press, Cambridge, New York, 1999).
- [9] C. Cohen-Tannoudji, B. Diu, and F. Laloë, *Quantum Mechanics. Volume 1: Basic Concepts, Tools, and Applications*, 2nd ed. (Wiley-VCH Verlag GmbH & Co. KGaA, Weinheim, 2020).
- [10] N. Rivera, I. Kaminer, B. Zhen, J. D. Joannopoulos, and M. Soljačić, Shrinking light to allow forbidden transitions on the atomic scale, *Science* **353**, 263 (2016).
- [11] M. L. Andersen, S. Stobbe, A. S. Sørensen, and P. Lodahl, Strongly modified plasmon-matter interaction with mesoscopic quantum emitters, *Nat. Phys.* **7**, 215 (2011).
- [12] P. Tighineanu, M. L. Andersen, A. S. Sørensen, S. Stobbe, and P. Lodahl, Probing Electric and Magnetic Vacuum Fluctuations with Quantum Dots, *Phys. Rev. Lett.* **113**, 043601 (2014).
- [13] P. Tighineanu, A. S. Sørensen, S. Stobbe, and P. Lodahl, Unraveling the Mesoscopic Character of Quantum Dots in Nanophotonics, *Phys. Rev. Lett.* **114**, 247401 (2015).
- [14] Y. Zhang, Z.-C. Dong, and J. Aizpurua, Influence of the chemical structure on molecular light emission in strongly localized plasmonic fields, *J. Phys. Chem. C* **124**, 4674 (2020).
- [15] N. Rivera and I. Kaminer, Light-matter interactions with photonic quasiparticles, *Nat. Rev. Phys.* **2**, 538 (2020).
- [16] M. Soljačić and J. D. Joannopoulos, Enhancement of nonlinear effects using photonic crystals, *Nat. Mater.* **3**, 211 (2004).
- [17] D. Dovzhenko, V. Krivenkov, I. Kriukova, P. Samokhvalov, A. Karaulov, and I. Nabiev, Enhanced spontaneous emission from two-photon-pumped quantum dots in a porous silicon microcavity, *Opt. Lett.* **45**, 5364 (2020).
- [18] P. K. Jain, D. Ghosh, R. Baer, E. Rabani, and A. P. Alivisatos, Near-field manipulation of spectroscopic selection rules on the nanoscale, *Proc. Natl. Acad. Sci. USA* **109**, 8016 (2012).
- [19] A. M. Kern and O. J. F. Martin, Strong enhancement of forbidden atomic transitions using plasmonic nanostructures, *Phys. Rev. A* **85**, 022501 (2012).
- [20] V. Yannopoulos and E. Paspalakis, Giant enhancement of dipole-forbidden transitions via lattices of plasmonic nanoparticles, *J. Mod. Opt.* **62**, 1435 (2015).
- [21] F. Marquier, C. Sauvan, and J.-J. Greffet, Revisiting quantum optics with surface plasmons and plasmonic resonators, *ACS Photonics* **4**, 2091 (2017).
- [22] S. Sanders, A. May, A. Alabastri, and A. Manjavacas, Extraordinary enhancement of quadrupolar transitions using nanostructured graphene, *ACS Photonics* **5**, 3282 (2018).
- [23] J. Sloan, N. Rivera, J. D. Joannopoulos, I. Kaminer, and M. Soljačić, Controlling spins with surface magnon polaritons, *Phys. Rev. B* **100**, 235453 (2019).
- [24] D. S. Wang, T. Neuman, and P. Narang, Spin emitters beyond the point dipole approximation in nanomagnonic cavities, *J. Phys. Chem. C* **125**, 6222 (2021).
- [25] N. Rivera, G. Rosolen, J. D. Joannopoulos, I. Kaminer, and M. Soljačić, Making two-photon processes dominate one-photon processes using mid-IR phonon polaritons, *Proc. Natl. Acad. Sci. USA* **114**, 13607 (2017).
- [26] N. Rivera, T. Christensen, and P. Narang, Phonon polaritons in two-dimensional materials, *Nano Lett.* **19**, 2653 (2019).
- [27] T. Neuman, R. Esteban, D. Casanova, F. J. García-Vidal, and J. Aizpurua, Coupling of molecular emitters and plasmonic cavities beyond the point-dipole approximation, *Nano Lett.* **18**, 2358 (2018).
- [28] E. Rusak, J. Straubel, P. Gładysz, M. Göddel, A. Kędziorski, M. Kühn, F. Weigend, C. Rockstuhl, and K. Słowik, Enhancement of and interference among higher order multipole transitions in molecules near a plasmonic nanoantenna, *Nat. Commun.* **10**, 5775 (2019).
- [29] M. Kosik, O. Burlayenko, C. Rockstuhl, I. Fernandez-Corbaton, and K. Słowik, Interaction of atomic systems with quantum vacuum beyond electric dipole approximation, *Sci. Rep.* **10**, 5879 (2020).
- [30] G. Rosolen and B. Maes, Strong multipolar transition enhancement with graphene nanoislands, *APL Photonics* **6**, 086103 (2021).
- [31] M. Göppert-Mayer, Über Elementarakte mit zwei Quantensprüngen, *Ann. Phys. (Berlin, Ger.)* **401**, 273 (1931).
- [32] G. Breit and E. Teller, Metastability of hydrogen and helium levels., *Astrophys. J.* **91**, 215 (1940).
- [33] L. J. Spitzer and J. L. Greenstein, Continuous emission from planetary nebulae, *Astrophys. J.* **114**, 407 (1951).
- [34] H. Krüger and A. Oed, Measurement of the decay-probability of metastable hydrogen by two-photon emission, *Phys. Lett. A* **54**, 251 (1975).
- [35] S. P. Goldman and G. W. F. Drake, Relativistic two-photon decay rates of $2s_{1/2}$ hydrogenic ions, *Phys. Rev. A* **24**, 183 (1981).
- [36] Y. Ota, S. Iwamoto, N. Kumagai, and Y. Arakawa, Spontaneous Two-Photon Emission from a Single Quantum Dot, *Phys. Rev. Lett.* **107**, 233602 (2011).
- [37] A. Hayat, P. Ginzburg, and M. Orenstein, High-rate entanglement source via two-photon emission from semiconductor quantum wells, *Phys. Rev. B* **76**, 035339 (2007).
- [38] A. Hayat, P. Ginzburg, and M. Orenstein, Observation of two-photon emission from semiconductors, *Nat. Photonics* **2**, 238 (2008).
- [39] H. M. van Driel, On the path to entanglement, *Nat. Photonics* **2**, 212 (2008).
- [40] A. Nevet, N. Berkovitch, A. Hayat, P. Ginzburg, S. Ginzach, O. Sorias, and M. Orenstein, Plasmonic nanoantennas for broad-band enhancement of two-photon emission from semiconductors, *Nano Lett.* **10**, 1848 (2010).

- [41] F. Hu, L. Li, Y. Liu, Y. Meng, M. Gong, and Y. Yang, Two-plasmon spontaneous emission from a nonlocal epsilon-near-zero material, *Commun. Phys.* **4**, 84 (2021).
- [42] A. N. Poddubny, P. Ginzburg, P. A. Belov, A. V. Zayats, and Y. S. Kivshar, Tailoring and enhancing spontaneous two-photon emission using resonant plasmonic nanostructures, *Phys. Rev. A* **86**, 033826 (2012).
- [43] A. Hayat, A. Nevet, P. Ginzburg, and M. Orenstein, Applications of two-photon processes in semiconductor photonic devices: Invited review, *Semicond. Sci. Technol.* **26**, 083001 (2011).
- [44] A. Hayat, P. Ginzburg, and M. Orenstein, Entangled photon spectroscopy and communications based on semiconductor two-photon process, in *International Conference on Quantum Information* (OSA, Rochester, New York, 2007), p. JWC63.
- [45] J. Zhang, J. Ma, M. Parry, M. Cai, R. Camacho-Morales, L. Xu, D. N. Neshev, and A. A. Sukhorukov, Spatially entangled photon pairs from lithium niobate nonlocal metasurfaces, *Sci. Adv.* **8**, eabq4240 (2022).
- [46] J. E. Ehrlich, X. L. Wu, I.-Y. S. Lee, Z.-Y. Hu, H. Röckel, S. R. Marder, and J. W. Perry, Two-photon absorption and broadband optical limiting with bis-donor stilbenes, *Opt. Lett.* **22**, 1843 (1997).
- [47] Y. Muniz, F. S. S. da Rosa, C. Farina, D. Szilard, and W. J. M. Kort-Kamp, Quantum two-photon emission in a photonic cavity, *Phys. Rev. A* **100**, 023818 (2019).
- [48] Y. Muniz, A. Manjavacas, C. Farina, D. A. R. Dalvit, and W. J. M. Kort-Kamp, Two-Photon Spontaneous Emission in Atomically Thin Plasmonic Nanostructures, *Phys. Rev. Lett.* **125**, 033601 (2020).
- [49] See Supplemental Material at <http://link.aps.org/supplemental/10.1103/PhysRevA.107.063516> for detailed derivations of the two-photon spontaneous emission rate, of the relation between the two-photon spontaneous emission rates and Purcell factors, and of the multipolar second-order transition moments for a hydrogen atom.
- [50] D. P. Craig and T. Thirunamachandran, *Molecular Quantum Electrodynamics: An Introduction to Radiation-Molecule Interactions* (Academic Press, London, Orlando, 1984).
- [51] L. D. Barron and C. G. Gray, The multipole interaction Hamiltonian for time dependent fields, *J. Phys. A: Math., Nucl. Gen.* **6**, 59 (1973).
- [52] P. W. Milonni, *The Quantum Vacuum: An Introduction to Quantum Electrodynamics* (Academic Press, Boston, 1994).
- [53] C. Cohen-Tannoudji, B. Diu, and F. Laloë, *Quantum Mechanics. Volume 3: Fermions, Bosons, Photons, Correlations and Entanglement*, 1st ed. (Wiley-VCH GmbH & Co. KGaA, Weinheim, 2020).
- [54] J. D. Jackson, *Classical Electrodynamics*, 3rd ed. (Wiley, New York, 1999).
- [55] A. Zangwill, *Modern Electrodynamics* (Cambridge University Press, Cambridge, 2013).
- [56] S. Y. Buhmann, *Dispersion Forces I*, Springer Tracts in Modern Physics (Springer, Berlin, Heidelberg, 2012), Vol. 247.
- [57] J.-M. Jin, *The Finite Element Method in Electromagnetics*, 3rd ed. (John Wiley & Sons Inc, Hoboken, New Jersey, 2014).
- [58] A. Taflov and S. C. Hagness, *Computational Electrodynamics: The Finite-Difference Time-Domain Method*, 3rd ed., Artech House antennas and propagation library (Artech House, Boston, 2005).
- [59] M. C. Bottorff, G. J. Ferland, and J. P. Straley, Two-photon transitions and continuous emission from hydrogenic species, *Publ. Astron. Soc. Pac.* **118**, 1176 (2006).
- [60] R. D. Cowan, *The Theory of Atomic Structure and Spectra*, Los Alamos Series in Basic and Applied Sciences No. 3 (University of California Press, Berkeley, 1981).
- [61] S. Thongrattanasiri, F. H. L. Koppens, and F. J. García De Abajo, Complete Optical Absorption in Periodically Patterned Graphene, *Phys. Rev. Lett.* **108**, 047401 (2012).
- [62] Z. Fang, S. Thongrattanasiri, A. Schlather, Z. Liu, L. Ma, Y. Wang, P. M. Ajayan, P. Nordlander, N. J. Halas, and F. J. García De Abajo, Gated tunability and hybridization of localized plasmons in nanostructured graphene, *ACS Nano* **7**, 2388 (2013).
- [63] A. D. Kondorskiy, N. T. Lam, and V. S. Lebedev, Absorption and scattering of light by silver and gold nanodisks and nanoprisms, *J. Russ. Laser Res.* **39**, 56 (2018).
- [64] J. Feng, Y.-F. Liu, Y.-G. Bi, and H.-B. Sun, Light manipulation in organic light-emitting devices by integrating micro/nano patterns: Light manipulation in organic light-emitting devices by integrating micro/nano patterns, *Laser Photonics Rev.* **11**, 1600145 (2017).
- [65] G. P. Agrawal, *Nonlinear Fiber Optics*, 4th ed., Quantum Electronics—Principles and Applications (Elsevier/Academic Press, Amsterdam, Boston, 2007).
- [66] Y. Zeng, Y. Fu, X. Chen, W. Lu, and H. Ågren, Highly efficient generation of entangled photon pair by spontaneous parametric downconversion in defective photonic crystals, *J. Opt. Soc. Am. B* **24**, 1365 (2007).
- [67] A. Dousse, J. Suffczyński, A. Beveratos, O. Krebs, A. Lemaître, I. Sagnes, J. Bloch, P. Voisin, and P. Senellart, Ultrabright source of entangled photon pairs, *Nature (London)* **466**, 217 (2010).